national accelerator laboratory

THE IMPACT PICTURE FOR STRONG INTERACTIONS

J. K. Walker

April 1973

Abstract: A brief discussion of the general charac-
teristics of the Impact Picture is given. This leads
to a description of a phenomenological model of hadron
scattering which on the one hand satisfies the impact
picture at extremely high energies and on the other
successfully describes the data above 20 GeV in the
laboratory. In addition, many predictions on the gen-
eral behavior of high energy hadron-hadron interactions
are given.

Submitted to Rencontre de Moriond
Conference, Meribel-les-Allues,
France, March 3-15, 1973

I. Introduction

In the last five years a profound advance has occurred in our understanding of the asymptotic high energy behavior of relativistic quantum field theories. Much of the progress in this area has been achieved by H. Cheng and T. T. Wu. They have shown that a variety of field theories have the same general feature in the limit of extremely high energies. The solution satisfies all honored physical principles such as unitarity, analyticity, and crossing symmetry.

The central question is: Does this solution apply to the strong interactions of hadrons? The test will and must come from experiments. The recent accurate measurements of proton-proton total cross sections at the ISR give strong support to the impact picture. It is, therefore, worthwhile to make a preliminary appraisal of the experimental situation at this time, when a great many new experiments will shortly be completed at the National Accelerator Laboratory, USA, and the Intersecting Storage Ring at CERN. The purpose of this paper is threefold. First, to provide an experimentalists viewpoint of the theoretical progress of the last few years in this field. As such, it embraces a lack of rigor. However, it is hoped that it provides some inspiration and understanding to experimentalists about this particular theoretical interpretation of their data. Secondly, I will report on a preliminary analysis of existing high energy data using a phenomenological model which on the one hand possesses all properties demanded by the impact picture at extremely high energies and, on the other hand, is sufficiently realistic to fit data for incident laboratory energy above 20 GeV. Finally, I will briefly present other predictions of the impact picture.

II. Theoretical Basis of the Impact Picture

Most of the theoretical effort has been devoted to a study of quantum electrodynamics with massive photons at very high energy. General features of the high energy scattering amplitudes have emerged. It has been verified that the same general features occur with scalar quantum electrodynamic field theory and ϕ^3 theory. We shall confine our attention to quantum electrodynamics.

High Energy Limit of Elastic Scattering

Consider the elastic process

$$a + b \rightarrow a + b$$

in the limit

$$s \rightarrow \infty$$

and t fixed.

The relevant lowest order diagrams for the three processes are shown below with their corresponding dependences on energy.

Process	s^0	s	$i\, s$
e + e → e + e			
γ + e → γ + e			
γ + γ → γ + γ			

Only examples of the diagrams are shown at any given order.

At high enough order the Amplitude $\propto i\, s$. Hence

$$\lim_{s \rightarrow \infty} \sigma_T \text{ is finite and non-zero.}$$

Thus cross sections tend to constants to this order in the expansion.

A general feature turns out to be that for the important diagrams photons are exchanged between groups of particles which may be the incident particles themselves or the ones created by them.

Higher Orders

We inquire whether if we go to still higher order are there terms that grow faster than s as $s \rightarrow \infty$. In this case the result would be

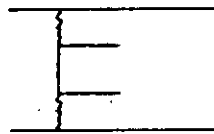$$\lim_{s \to \infty} \sigma_T \to \infty$$

Consider again ee -- going to higher order

The amplitude in this case goes as $i \, s \, \ell ns$. In general, it turns out that electron loops give $s \, \ell ns$ terms.

By the Optical Theorem the above diagram is related to

} the production of low energy particles in cms (in hadron physics referred to as pionization)

Given that there are diagrams that grow faster than s, a vital question poses itself: What happens after we sum all diagrams that give logarithmic factors? e.g.,
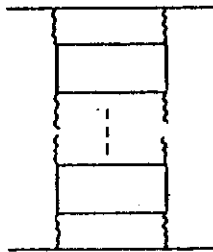
In this case, n loops lead to $i \, \alpha^{2(n+1)} \, s (\ell ns)^n$.

Summing over all possibilities gives the result

$$amp \propto \frac{i \, s^{1+c}}{(\ell ns)^2}$$

where $c = \frac{11\pi \, \alpha^2}{32}$ for QED and similar results for scalar electrodynamics, ϕ^3 theory, etc. In general, c is related to a coupling constant in the theory. The exponent of the ℓns term in the denominator seems to be probably ≥ 1 in general. Thus the amplitude increases faster than s (for this class of diagrams). At first sight this is a disturbing result and appears to lead to a total cross section that rises as a power of s. This possibility would violate the Froissart bound. We will now discuss the solution to this dilemma.

We express the scattering amplitude in the impact-distance representation.

$$M(s,-\Delta^2) = \frac{is}{2\pi} \int dx_\perp \, e^{i \vec{\Delta} \cdot \vec{x}_\perp} D(s,x_\perp)$$

where now $M(s,-\Delta^2)$ includes contributions from ALL possible diagrams in the world.

$D(s,x_\perp)$ is defined to be the opacity at s and $x_\perp$. By a Fourier Transform we obtain

$$D(s,x_\perp) \sim s^{-1} \int d^2 \Delta^2 \, e^{-i \vec{\Delta} \cdot \vec{x}_\perp} M(s,-\Delta^2) \, .$$

In the limit of large $x_\perp$, we replace $M(s,-\Delta^2)$ by

$$\frac{1}{-\Delta^2 - \lambda^2}$$

which is the form of the propagator for the exchange of a particle. We then obtain

$$D(s,x_\perp) \sim \exp(-\lambda |x_\perp|) \, .$$

Thus the smallest effective λ contributes most to $D(s,x_\perp)$ at large $x_\perp$. This is all consistent with our intuitive understanding. The leading diagrams of this kind are just the kind of diagrams that we have discussed and have, in addition, the s dependence given previously.
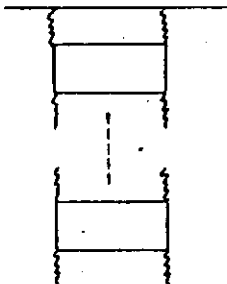
Thus at large $x_\perp$ we have the important result that

$$D(s,x_\perp) \sim \frac{s^c}{(\ell ns)^2}\ e^{-\lambda\ |x_\perp|}\ .$$

Now consider the case of fixed large $x_\perp$, then $D(s,x_\perp)$ increases with s.

Thus the <u>interaction extends into larger and larger transverse distances</u> <u>as s increases</u>. Thus $D(s,x_\perp)$ approaches 1, at a value of s such that

$$\boxed{\frac{c}{\lambda}\ \ell ns \equiv R \geqslant |x_\perp|\ .}$$

Other diagrams become important in that case.

The most general statement seems to be that

$$D(s,x_\perp)\Big|_{x_\perp \leqslant R} \quad \xrightarrow{\ s\,\to\,\infty\ } \quad \text{Constant}$$

The constant may or may not be as large as unity. However, it seems natural that for strong interactions the constant should be as large as possible, namely unity.

The picture which emerges is that a particle acts like a Lorentz contracted pancake with two regions
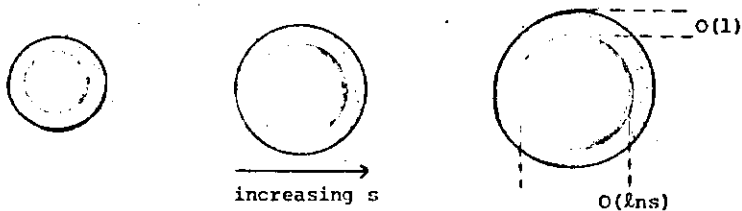

There is a gray fringe area and in the center there is a black core.

III. -1) The Phenomenological Model

In association with Cheng and Wu an effort has been made to construct a phenomenological model that possesses the above properties of the impact picture and yet at the same time is sufficiently realistic to fit the data from Serpukhov, NAL, and the ISR.

We want $D(s,x_\perp)$ to look like
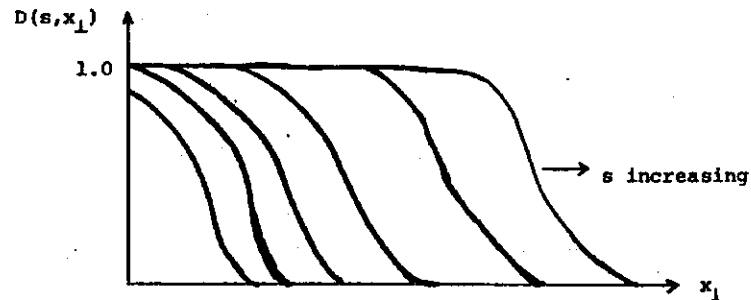
The simplest form is

$$D(s,x_\perp) = 1 - \exp\left[-S(s)\ F(x_\perp^2)\right].$$

The function $S(s)$ will be the same for <u>all</u> processes mediated by the Pomeron, e.g.

$$\pi + p \to \pi + p$$

and $\qquad p + p \to p + p$.

All channel information resides in $F_j(x_\perp^2)$ for j^{th} channel. We take

$$F_j(x_\perp^2) = f_j\ \exp\left[-\lambda(x_\perp^2 + x_{oj}^2)^{1/2}\right].$$

This involves three parameters: f_j, λ, x_{oj}. λ does not depend on the channel because for large $x_\perp$

$$F_j \sim \exp(-\lambda\ x_\perp)$$

and the shape of the opacity function at the fringe should be a property of the pomeron – not of the channel.

On the basis of our experience with QED we might take

$$S(s) = \frac{s^c}{(\ell ns)^{c'}} .$$

For the present, however, it is an adequate approximation to take $c' = 0$ thereby obtaining a value for an "effective" c. The asymptotic energy scale of hadron interactions is then controlled by the value of c. There is a problem with the choice $S(s) = s^c$. In this case the elastic scattering amplitudes for the two processes

$$a + b \rightarrow c + d$$

and $\quad \overline{a} + b \rightarrow \overline{c} + d \quad$ are not equal.

i.e. we demand that the amplitude satisfy crossing which it clearly does not with the above choice of S(s).

Consider the complex s plane.
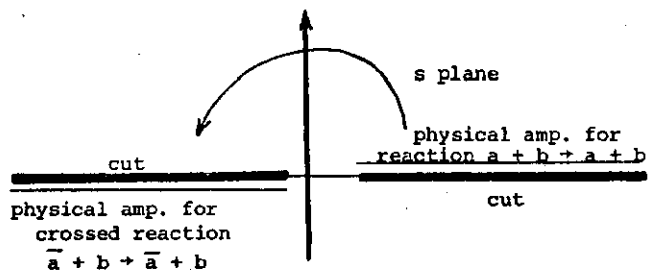
We require that if we analytically continue the direct amplitude to the position of the other amplitude then this function should describe the crossed reaction. The choice

$$S(s) = \left[s \exp(-i\ \pi/2) \right]^c$$

achieves this.

The model then has the elastic scattering amplitudes

$$M_j(s,-\Delta^2) \text{ functions of } x_{oj},\ f_j,$$

which depend on the channel and two real constants λ and c which are common to all channels.

The differential cross section for elastic scattering in channel j is (in the limit of large s)

$$\frac{d\sigma}{dt}\ (j) = \left| \frac{M_j(s,-\Delta^2)}{s} \right|^2 \tag{1}$$

where $t = -\Delta^2$.

The total cross section is related to the imaginary part of $M_j(s,0)$

$$\sigma_{total}\ (j) = \frac{4\pi}{s}\ Im\ M_j(s,0).$$

[Remember that to convert from $(GeV)^{-2}$ to mb, a factor of $\frac{4.893}{4\pi}$ is needed.]

As Im $M(s,0)/s$ is an increasing function of s, the total cross sections will rise. If total cross sections do rise indefinitely with energy, at what energy does this begin to occur? Until very recently, the data of Denisov et al. at Serpukhov for the K^+p channel, was the only case of an appreciable rise in total cross section. There is some reason to expect that an exotic channel may show asymptotic features at a lower energy than for a non-exotic channel. In order to determine the value of c, one accurate piece of data is required at very high energy. Very recently, this most important piece of information has been provided by two beautiful experiments at the ISR in the form of a total pp cross section. At lower energies we assume the increase is masked by a decreasing background. In this case we assume

$$\sigma_{total}\ (j) = A_j\ s^{-1/2} + \frac{4\pi}{s}\ Im\ M_j(s,0). \tag{2}$$

In order to satisfy the optical theorem, this parameter A_j should appear also in the formula for $d\sigma/dt$. However, at this stage we have concentrated on trying to take proper account only of the pomeron (or asymptotic) contribution to $d\sigma/dt$.

This completes the description of our simple model for all asymptotic hadronic processes. Later we shall generalize it to inelastic diffraction scattering without spin-parity exchange.

III. -2) Properties of the Model

The function $F_j(x_\perp^2)$ has the property that, raised to an arbitrary positive power, the two-dimensional Fourier transform is an elementary function. More precisely

$$(2\pi)^{-1} \int d\vec{x}_\perp e^{-i \vec{\Delta} \cdot \vec{x}_\perp} \left[F_j(x_\perp^2)\right]^n$$

$$= f_j^n \ n \ \lambda \left[1 + x_{oj}(\Delta^2 + n^2\lambda^2)^{1/2}\right] (\Delta^2 + n^2\lambda^2)^{-3/2}$$

$$\exp\left[-x_{oj}(\Delta^2 + n^2\lambda^2)^{1/2}\right] \tag{3}$$

for $n > 0$.

We then obtain, after expanding $D(s,x_\perp)$

$$M_j(s,-\Delta^2) = i \ s \ \lambda \sum_{n=1}^{\infty} \frac{(-1)^{n-1} f_j^n \left[s \exp(-i \ \pi/2)\right]^{nc}}{(n-1)!}$$

$$\left[1 + x_{oj}(\Delta^2 + n^2\lambda^2)^{1/2}\right] (\Delta^2 + n^2\lambda^2)^{-3/2}$$

$$\exp\left[-x_{oj}(\Delta^2 + n^2\lambda^2)^{1/2}\right]. \tag{4}$$

Equations (1), (2), (3), and (4) give completely the model.

Of course in this asymptotic model

$$\frac{d\sigma}{dt}(\bar{h}h) = \frac{d\sigma}{dt}(hh)$$

where h is any hadron. Since we have at the present time omitted from $d\sigma/dt$ the background terms which fall presumably approximately as some power of s, our values of $d\sigma/dt$ should be most accurate for K^+p and then less accurate in order for pp, π^+p, π^-p, K^-p, and $\bar{p}p$.

III. -3) Numerical Analysis

Our objective is to provide a reasonable numerical fit to all hadron-hadron processes at high energies $s \gtrsim 40$ GeV^2. The fit should improve for the higher energy data.

It is worthwhile to clearly state the number of parameters in the fit. The total cross sections are parameterized in the form

$$\sigma_{total}(j) = A_j \ s^{-1/2} + \frac{4\pi}{s} \ \text{Im} \ M_j(s,0).$$

This involves six constants A_j (for the channels p, $\bar{p}$, π^+, π^-, K^+, K^-). In addition, M_j involves two parameters f_j and x_{oj} which depend on the channel but are the same for particle and antiparticle. This produces an additional six parameters. Finally, there are two parameters which are independent of the channel. The first of these λ, characterize the shape of the fringe of the interaction region. The other parameter c establishes the energy scale in asymptotic hadron dynamics.

This involves a total of 14 parameters, the six A_j help fit the total cross sections at low energies ($40 \lesssim s \lesssim 100$), thereby yielding better information on the asymptotic part of the cross section. Above $s \approx 100$ essentially all of our fits and predictions for total cross sections, elastic and inelastic diffractive cross sections, for all channels are determined by the remaining eight parameters.

Specifically the above fourteen parameters are determined from the following fourteen pieces of data:

1) At E = 20 BeV, the pp total cross section is 39.0 mb.

2) At E = 60 BeV, the pp total cross section is 38.4 mb.

3) At E = 1485 BeV, the pp total cross section is 43.2 mb. This is the crucial piece of data obtained at the ISR to which we have previously referred.

4) At E = 60 BeV, the dip in the pp differential cross section occurs at $|t| = 1.8$ (BeV/c)^2. This value is somewhat arbitrary.

5) At E = 505 BeV, the average slope, between $|t|$ of 0.14 and 0.24 (BeV/c)^2, for $\ell n \ d\sigma/dt$ is 11.5 (BeV/c)$^{-2}$ for pp elastic scattering.

6) At E = 20 BeV, the total K⁺p cross section is 17.5 mb.

7) At E = 60 BeV, the total K⁺p cross section is 18.3 mb.

8) At E = 60 BeV, the average slope, between $|t|$ of 0.1 and 0.28 $(BeV/c)^2$, for $\ell n \, d\sigma/dt$ is 7.4 $(BeV/c)^{-2}$ for K⁺p elastic scattering.

9) At E = 47.5 BeV, the $\overline{p}p$ total cross section is 44.1 mb.

10) At E = 52.5 BeV, the K⁻p total cross section is 20.3 mb.

11) At E = 20 BeV, the π⁺p total cross section is 23.5 mb.

12) At E = 60 BeV, the π⁺p total cross section is 23.15 mb.

13) At E = 54.2, the average slope, between $|t|$ of 0.05 and 0.53 $(BeV/c)^2$, for $\ell n \, d\sigma/dt$ is 9.5 $(BeV/c)^{-2}$ for π⁺p elastic scattering.

14) At E = 60 BeV, the π⁻p total cross section is 24.2 mb.

The resulting parameters are:

c	=	0.082925
λ	=	0.60071
$x_o(pp)$	=	3.8750
f(pp)	=	6.5812
A(pp)	=	47.372
$x_o(Kp)$	=	1.4295
f(Kp)	=	1.3452
$x_o(\pi p)$	=	3.8457
f(πp)	=	3.6355
A(π⁺p)	=	29.220
A($\overline{p}$p)	=	101.81
A(K⁺p)	=	8.2543
A(K⁻p)	=	29.384
A(π⁻p)	=	40.416

III.-4) Total Cross Sections

The existing total cross section data is shown in Fig. 1. There is, in addition, cosmic ray data which shows that the proton-proton cross section is rising in the range $10^4 \leq s \leq 10^6$ GeV.

We predict on the basis of this parameterization of the data that the positive pion, kaon, and proton cross sections will all rise measurably in the energy range available at NAL. Observations of this phenomenon will be of great interest and importance.

Elastic Scattering

Figure 2 shows the predictions for the elastic scattering of protons. A break at $|t|$ somewhere between 1 and 2 $(GeV/c)^2$ in the slope of $d\sigma/dt$ for proton-proton elastic scattering has been known for several years. The interesting feature of this break is that it tends to become more apparent as the incident energy is increased. This behavior is unique compared to other dips, bumps, shoulders, and structures in all channels of hadron-hadron scattering. Within the context of the impact picture, such structure in elastic differential cross sections must develop as the energy increases. This is due to the blackness of the core developing as energy increases and consequently a diffraction pattern with dips must become apparent. We predict two things; first the dip will become more pronounced as energy increases, and secondly, the position of the dip will move slowly to smaller values of momentum transfer as the energy is increased. These qualitative effects should all be observable at both the National Accelerator Laboratory and the ISR.

Recently, preliminary results on pion-proton elastic scattering at large momentum transfer have been reported by Orear et al. A distinct break in $d\sigma/dt$ occurs at $|t| \simeq 2.8$ $(GeV/c)^2$. Our fit successfully predicts a dip at $|t| \simeq 3$ $(GeV/c)^2$ for $s \lesssim 100$ $(GeV)^2$. As the energy is increased the dip develops slightly and its position moves to smaller momentum transfer much more rapidly than in the case of proton-proton elastic scattering. Early experiments in the Meson Laboratory at the

National Accelerator Laboratory will have the accuracy and sensitivity
to confirm these predictions for pion-proton scattering.

In the case of Kp elastic scattering we predict that there will be
no dip in the cross section. However, we predict that the Kp elastic
cross section for $|t| \gtrsim 2$ GeV^2 will be larger than the corresponding
cross sections for πp and pp scattering.

We consider now the elastic scattering at small momentum transfer.
We have investigated possible structure in our predicted cross section
$d\sigma/dt$ for elastic proton-proton scattering in the range $0 \lesssim |t| \lesssim 0.3$.
Specifically, we have fitted two straight lines to $\ln (d\sigma/dt)$ to deter-
mine the value of $|t| = |t|_{break}$ such that there is an optimum fit. The
result is that $|t|_{break} = 0.13 \pm 0.02$ (GeV/c)^2 in the range $10^2 \lesssim s \lesssim 10^6$.
In addition, for small changes of parameters given previously this result
still holds. A break at $|t| = 0.13$ in the slope of the elastic scatter-
ing cross section in proton-proton collisions therefore emerges in a
rather parameter-independent way. Our model correctly gives not only
the break at a reasonable place ($|t| \approx 0.13$) but also a value of Δb in
the range indicated by the experimental data.

Figure 3 shows the available data for b from Serpukhov and the ISR
on proton-proton elastic scattering. It can be seen that the rapid
shrinkage observed at Serpukhov appears to have slowed down for $s \gtrsim 100$
(GeV)^2. We predict a continuing slow shrinkage for $s > 100$ GeV^2 in both
ranges of momentum transfer.

High quality data on b from the USSR-American collaboration at NAL
studying proton-proton scattering for $40 \lesssim s \lesssim 800$ and in both ranges of
momentum transfer should be able to confirm these predictions.

We predict similar breaks in the πp and Kp differential cross sec-
tions. High precision (0.5%) measurements on b will be made in the
Meson Laboratory of the National Accelerator Laboratory for both pions
and kaons up to $s \approx 300$ (GeV)^2. The predicted slow shrinkage and breaks
should be able to be confirmed by these measurements.

III. -5) Inelastic Diffractive Scattering

Consider the scattering problem with N channels which are coupled
through diffractive processes. Let the scattering matrix element be
written in impact distance representation as

$$\sim i \int d\vec{x}_\perp \, e^{i \vec{\Delta} \cdot \vec{x}_\perp} [I + a(\vec{x}_\perp)]$$

where $a(\vec{x}_\perp)$ is an N x N matrix and I is the unit matrix.

It is important to realize that since all diffractive processes
are mediated by the same pomeron the effective "potential" involved has
the same range and energy dependence. The matrix $a(\vec{x}_\perp)$ describes the
scattering mediated by the pomeron and its diagonal elements represent
elastic scattering. Since the pomeron is relevant to all the processes,
all of the matrix elements of $a(\vec{x}_\perp)$ must be of the same order of magni-
tude. Since the very words "black core" mean that the diagonal matrix
elements of $a(\vec{x}_\perp)$ are small there, the off-diagonal elements of $a(\vec{x}_\perp)$
must also be small there. Thus we conclude

$$a_{ij}(\vec{x}_\perp) \approx 0, \qquad i,j = 1,2,\ldots N$$

inside the core.

Outside the black core, there is a grey fringe of thickness O(1).
By definition, the diagonal matrix elements of $a(\vec{x}_\perp)$ in the fringe are
O(1). Therefore in the fringe we have all elements of $a(\vec{x}_\perp)$ to be O(1).

$$a_{ij}(\vec{x}_\perp) = O(1), \quad i,j = 1,2,\ldots N.$$

Remembering that the unit matrix I is diagonal we see that the dominant
contribution to an elastic process comes from the black core. On the
other hand, the dominant contribution to a diffractive inelastic process
comes from the gray fringe.

Given that the radius of the black core grows as ℓns and the fringe
remains of constant width, we have

$$\frac{\sigma_{\text{elastic}}}{\sigma_{\text{diffractive elastic}}} = \frac{(\ell n s)^2}{(\ell n s)} \doteq \ell n s$$

in the limit of large s.

In terms of the previous parameterization of our model for elastic scattering the diagonal elements of $a(x_\perp)$, the simplest choice for the non-diagonal terms is

$$a_{ij}(s,\vec{x}_\perp) = C_{ij} \, S(s) \, F_{ij} \, (x_\perp^{\,2}) \, \exp\left[-S(s) \, F_{ij}(x_\perp^{\,2})\right]$$

where C_{ij} is a real constant and $S(s)$ and $F_{ij}(x_\perp^{\,2})$ are the same functions as defined for elastic scattering.

Using this form of $a_{ij}(s,\vec{x}_\perp)$ we obtain the matrix element for a diffractive inelastic process

$$M_{ij}(s,-\Delta^2) = i \, s \, \lambda \, C_{ij} \sum_{n=1}^{\infty} \frac{n(-1)^{n-1} \, f_{ij}^{\,n} \, \left[s \, \exp(-i\,\pi/2)\right]}{(n-1)!}$$

$$\left[1 + x_{oij}(\Delta^2 + n^2\lambda^2)^{1/2}\right] (\Delta^2 + n^2\lambda^2)^{-3/2}$$

$$\exp\left[-x_{oij}(\Delta^2 + n^2\lambda^2)^{1/2}\right].$$

There are no free parameters other than the overall normalization factor C_{ij}.

Using the previously determined parameters, Fig. 4 shows the predicted cross sections for the reactions:

$$p + p \to p + N^*(1470)$$

$$\pi + p \to \pi + N^*(1470)$$

$$K + p \to K + N^*(1470) \ .$$

In addition we show the experimental data for the reaction

$$p + p \to p + N^*(1400).$$

The calculated curve is for the reaction

$$p + p \to p + N^*(1470),$$

and we have normalized the cross section by choosing C_{ij}^2, for this channel equal to 0.1. The $N^*(1400)$ is shifted in mass relative to the $N^*(1470)$ which is well established in pion-nucleon phase shift analyses. The explanation for this mass shift is not clear. However, if our identification of these two structures being the same particle is correct, then, the steep slope $(b \approx 15)$ observed for this reaction is accounted for in the present model. We predict a dip in the cross section at $|t| \approx 0.5$ and furthermore a slow movement of the dip position as the energy is increased. The experimental data is suggestive of a distinct change in slope at $|t| \approx 0.5$, however, there are large systematic uncertainties in the data for $|t| \gtrsim 0.5$ and the situation is unclear at this time. The figure shows that we expect the slope of $d\sigma/dt$ for

$$\pi + p \to p + N^*(1470)$$

to be significantly less than for the corresponding reaction for incident protons. In addition, there should be dip structures or breaks in these reactions which tend to move fairly rapidly as s is increased.

These three inelastic diffractive channels with no exchange of spin and parity can be studied using the very high resolution strong focusing spectrometer presently being constructed in the Meson Laboratory of the National Accelerator Laboratory.

The degree to which this model satisfies factorization can be investigated at this stage. First, we have calculated the ratios of the following reactions:

$$R(pp) = \frac{p + p \rightarrow p + p}{p + p \rightarrow p + N^*(1400)}$$

and similarly for the πp and Kp channels. If factorization is valid then

$$\mathcal{R} = \frac{R(pp)}{R(Kp)} = \frac{R(\pi p)}{R(Kp)} = 1.$$

Figure 5 shows the predictions of the model as a function of momentum transfer $|t|$. It can be seen that at small $|t|$ the model predicts that to within about 5 to 10%, factorization should hold. At larger $|t|$ factorization continues to be good for the πp and Kp comparison. However, in the pp to Kp comparison there is a marked increase in the extent to which factorization is broken as $|t|$ is increased. Because the differential cross sections are heavily weighted to small $|t|$ the integrated cross sections satisfy factorization to better than about 15%. In addition, we find that the s dependence of $\mathcal{R}$ is extremely weak. Thus, our model is consistent with various experimental checks which show that factorization works to about 10 or 20% for integrated cross sections. However, this model indicates that in the region of the dip which develops at $|t| \simeq 0.5$ for the pp diffraction scattering, factorization should fail rather badly.

The dashed curves are the predictions of the model in the case where we have refitted the model to all of the data given previously, however, in this case we have chosen $c' = 1$ rather than $c' = 0$. The predictions of the model are not sensitive to these choices for c'.

III. -6) Real to Imaginary Part of Forward Scattering Amplitude

The model makes predictions for these ratios for all of the elastic and diffractive inelastic processes already discussed. We recall that in the model the total cross section for a channel j such as pp or $\overline{pp}$ is given by

$$\sigma_{total}(j) = A_j s^{-1/2} + \frac{4\pi}{s} \text{Im } M_j(s,o)$$

where $M_j(s,o)$ is defined earlier. Since crossing symmetry is properly taken into account in this model $M_j(s,o)$ is analytic in the upper half plane. It is thus simply a matter of extending the background term $A_j s^{-1/2}$ to complex values of s. If we neglect the masses compared with $\sqrt{s}$ then the ratio of the real to imaginary parts of the forward scattering amplitude is given by

$$\alpha = \frac{-A_{j'} s^{-1/2} + 4.893 \text{Re } M_j(s,o)}{A_j s^{-1/2} + 4.893 \text{Re } M_j(s,o)}$$

Here j' denotes the corresponding u channel. For example, if j is the pp channel, the j' is the $\overline{pp}$ channel.

In figures 6, 7 and 8, α is plotted in the range $10^2 < s < 10^4$ GeV^2 for pp, $\overline{pp}$, $\pi^{\pm} p$, $K^{\pm} p$. The solid lines are for the parameterization $c' = 0$ and the dashed lines are for the case $c' = 1$. The difference between the two sets of curves is quite small. Of course, both sets of curves depend sensitively on the values of the recently measured total pp cross sections at the I.S.R. Figure 1 shows the experimental data for the pp channel from Serpukhov and the I.S.R. The agreement is quite satisfactory.

For s below 100 GeV^2, it is necessary to use the experimental data at lower energies and perform the dispersion integral. For s above 10^4 GeV^2 the two sets of curves are not in good agreement. Qualitatively, all α's approach zero slowly from positive values. For the two sets of curves the value of c is quite different. For $c' = 0$, $c = 0.08$ and for $c' = 1$, $c = 0.2$. Since we expect c to be less than 1 on very general grounds both values of c are acceptable. However, the choice $c' = 1$ and $c = 0.2$ is perhaps to be preferred. Since we are dealing with strong

interactions and c is related to the coupling constant, the larger value
of c appears preferably. In addition, in field theories studied so far,
it appears that $c' \gtrsim 1$, which lends support to the larger value of c.
The only channel which has been experimentally investigated at high energy
is once again the pp elastic. The ratio is predicted to increase from a
negative value at Serpukhov energies then crosses through zero at
s < 1000 and becomes positive. The recent data from the ISR is consistent
with this behavior. At higher energies the ratio is predicted to have
a broad maximum of around +0.1 in the region $10^4 \leqslant s \leqslant 10^5$ and then to
fall asymptotically to zero with a $(\log s)^{-1}$ dependence.

III. -7) Ratio of Elastic to Total Cross Section

In the limit of very high s where the black core dominates in its
contribution to the elastic scattering amplitude we expect

$$\sigma_{e\ell}/\sigma_{Tot} \to 1/2.$$

On the one hand our phenomenological model of the impact picture
fits this requirement, and on the other hand, it is clear from the
preceding discussion that the model fits the present values of
$\sigma_{e\ell}/\sigma_{Tot} \approx 0.17$ measured at the ISR. The predicted rate of increase of
this ratio, $\sigma_{e\ell}/\sigma_T$ from the present value of 0.17 to the asymptotic
value of 0.5 is very low. For example at $s \approx 10^6$ the ratio is still not
more than about 0.25. It is a fact that some functions approach their
limiting values more slowly than other functions!

IV. Other Predictions of the Impact Picture

IV. -1) Pionization

In Section II we mentioned the relationship between the increase
of total cross sections with energy and the production of slow particles
in the center of mass system. The impact picture provides this corre-
lation between these two phenomena in a quite precise way. There is no
way out of the dilemma for the impact picture if

a) one or other of the two phenomena do not exist,

b) the s dependence of the two phenomena are not correlated.

We have previously discussed the existence of rising total cross
sections. Experimentally, there is now also evidence from the ISR that
pions are produced with low momentum in the center of mass system and in
accord with the predicted distribution

$$\frac{d^3 p}{E} f(p_\perp^2) \left[\ell ns \right]^n \times s^q$$

where q is related to c and is positive.

Figure 9 shows the data for the reaction $p + p \to \pi + $ Anything.
The above distribution leads to a flat distribution in rapidity as
observed. Secondly, we expect a rise in the cross section for this
pionization as s is increased in the range of the ISR where the total
cross section begins to increase. Figure 10 shows the available data.
The situation is not clear at this time as the accuracy of the data is
not very good. However, a rise is suggested by the data.

The approach to the asymptotic s dependence in the central region
predicted by this model is surely going to be slow. Not only is this
suggested by Mueller type arguments, but more convincingly, the present
data on the π^-/π^+ ratio in the central region at ISR energies is
approaching 1 rather slowly. Hence it will be difficult to make a
convincing comparison of the predicted and observed s dependence of
pionization in the central region at available ISR energies. Clearly,
a higher energy storage ring would be very useful in this regard.

There are of course many ways to saturate the Froissart bound.
However, the connection between the total cross section and pionization
is a key stone of the impact picture. Thus accurate data on this
process is of great importance to assess the relevance of the impact
picture.

Finally, in this connection, we should say that the predicted s^q
$\left[\log s \right]^n$ dependence should hold for any $p_\perp$ for large enough s.

IV. -2) Pionization in Exclusive Processes

The impact picture predicts that a similar distribution

$$\frac{d^3p}{E} \, f(p_\perp{}^2) \, \left[\ell ns\right]^m \qquad \text{(m \underline{negative})}$$

should hold for exclusive processes with suitable quantum numbers. For example the above distribution should hold for the reaction

$$p + p \rightarrow \pi^+ + \pi^- + p + p.$$

Thus for this exclusive channel there should be a flat rapidity distribution and in addition a $\left[\ell ns\right]^m$ energy dependence. There is already some experimental evidence for both of the effects.

V. Conclusions

We have made a preliminary appraisal of the relevance of the Impact Picture for high energy hadron interactions. The conclusions at this time are the following:

1) The prediction that total cross sections rise with energy is correct for two channels and represents a major qualitative triumph for the theory. Fairly firm predictions are now given for the other channels.

2) The predicted pionization has been found to exist. The energy dependence of this process has not yet been carefully checked and may prove difficult at existing energies.

3) The predicted development of diffraction minima in the elastic scattering has been found to take place. The predicted s dependence of the position of the minima in the cross section has not yet been checked.

4) The predicted slow shrinkage in the slope parameter (b) at high energy is in good agreement with the data.

5) Predictions for πp and Kp elastic scattering have yet to be fully tested. However, the predicted first diffraction minimum in the πp case at $|t| \simeq 3$ appears to have been seen experimentally.

6) Predictions for diffractive inelastic scattering in the various

channels have been given but there is little data to confront the predictions. The little data which exists is consistent with the theory. To a good approximation factorization is predicted for these channels at low momentum transfer.

7) The predicted real to imaginary ratio for the elastic pp amplitude is consistent with the data. Predictions are given for the phase of the $\pi^\pm$, $K^\pm$ forward scattering amplitudes.

Thus there is a fairly broad agreement between the predictions of the Impact Picture and the available data on the scattering of hadrons at high energy. Many new tests have been suggested here, which when completed will subject the Impact Picture to more detailed investigation. It is extremely encouraging at this time, however, that a single consistent theoretical picture seems to be emerging which on the one hand satisfies the fundamental tenets of field theory and on the other provides a unifying view of total cross sections, elastic cross section, and inclusive reactions for all channels in hadron physics. It remains a major challenge in the near future to subject this theory to further confrontations with experimental data.

I acknowledge many stimulating discussions with Professors H. Cheng and T. T. Wu.

Figure Captions

Fig. 1   Total hadron-proton cross sections in millibarns are shown as
a function of s (the square of the center-of mass energy). The
curves are predictions of the impact picture with the parameter-
ization given in the text.

Fig. 2   Proton-proton differential elastic scattering cross section
dσ/dt as a function of $|t|$ for various values of s. The solid
curves are predictions of the impact picture with the parameter-
ization given in the text.

Fig. 3   Values of the slope parameter b at small momentum transfer
$(0.05 \leqslant |t| \leqslant 0.15)$ and intermediate momentum transfer
$(0.15 \leqslant |t| \leqslant 0.35)$ are shown as a function of s. The curves
are the predictions of the impact picture with the parameter-
ization given in the text.

Fig. 4   Diffractive inelastic scattering without spin or parity exchange
for the pp, πp, and Kp channels. The solid curves are predic-
tions of the impact picture with the parameterization given in
the text. The chosen values of s are those possible at the ISR
and also with pion and kaon beams at the NAL and CERN II.

Fig. 5 $\mathcal{R} = \frac{R(hp)}{R(h'p)}$, where R(hp) is the ratio of the elastic to diffractive
inelastic channel, is plotted versus $|t|$ for s = 100 GeV^2.

Fig. 6   Real to imaginary part of the forward scattering amplitude for the
proton proton case. The solid and dashed curves are for the
cases c' = 0 and c' = 1 respectively.

Fig. 7   Real to imaginary part of the forward scattering amplitude for the
pion proton case. The solid and dashed curves are for the
cases c' = 0 and c' = 1 respectively.

Fig. 8   Real to imaginary part of the forward scattering amplitude for the
kaon proton case. The solid and dashed curves are for the
case c' = 0 and c' = 1 respectively.

Fig. 9   Rapidity Plot in the central region for pion production
in proton-proton collisions.

Fig. 10 Energy dependence of the 90 degree differential cross section
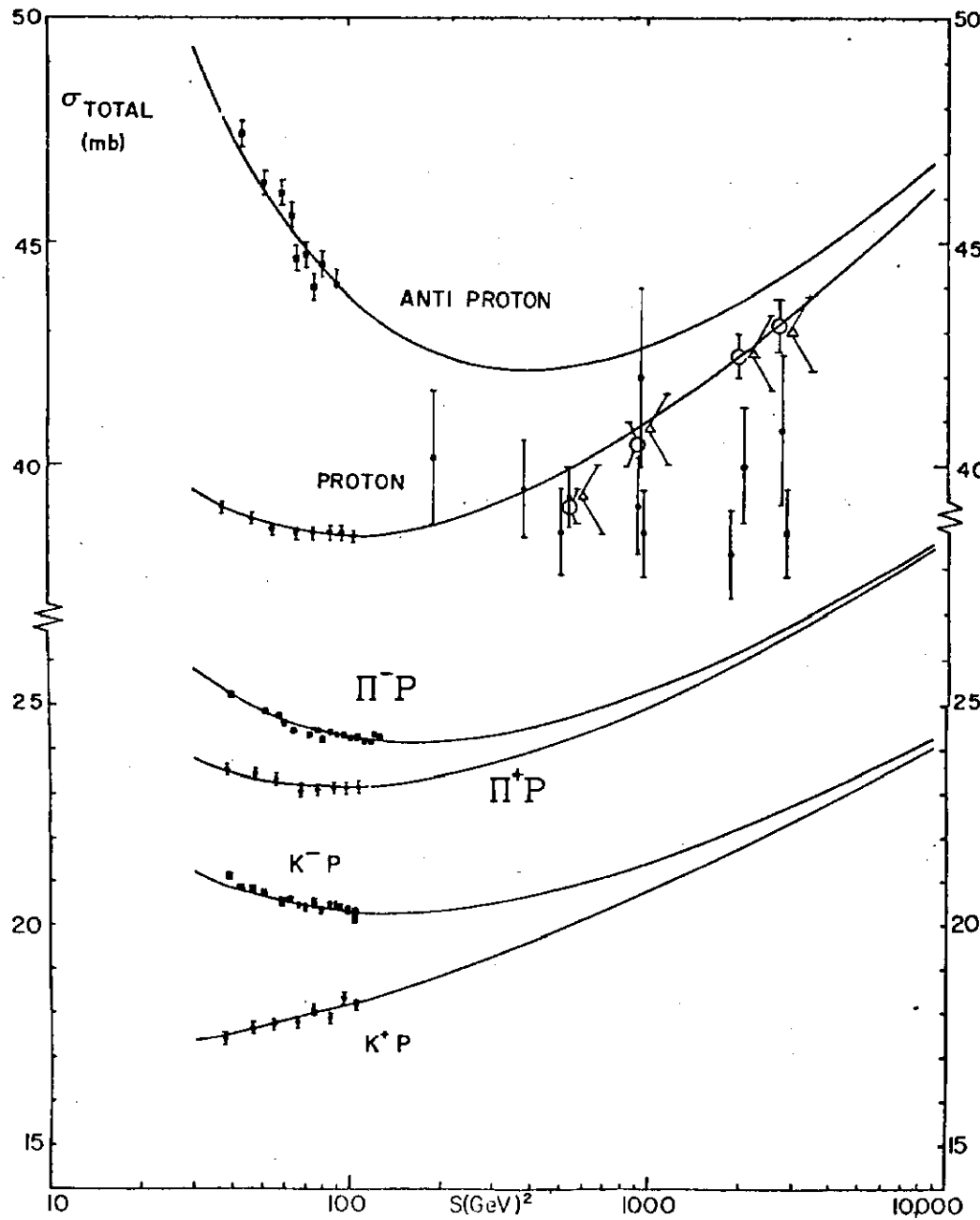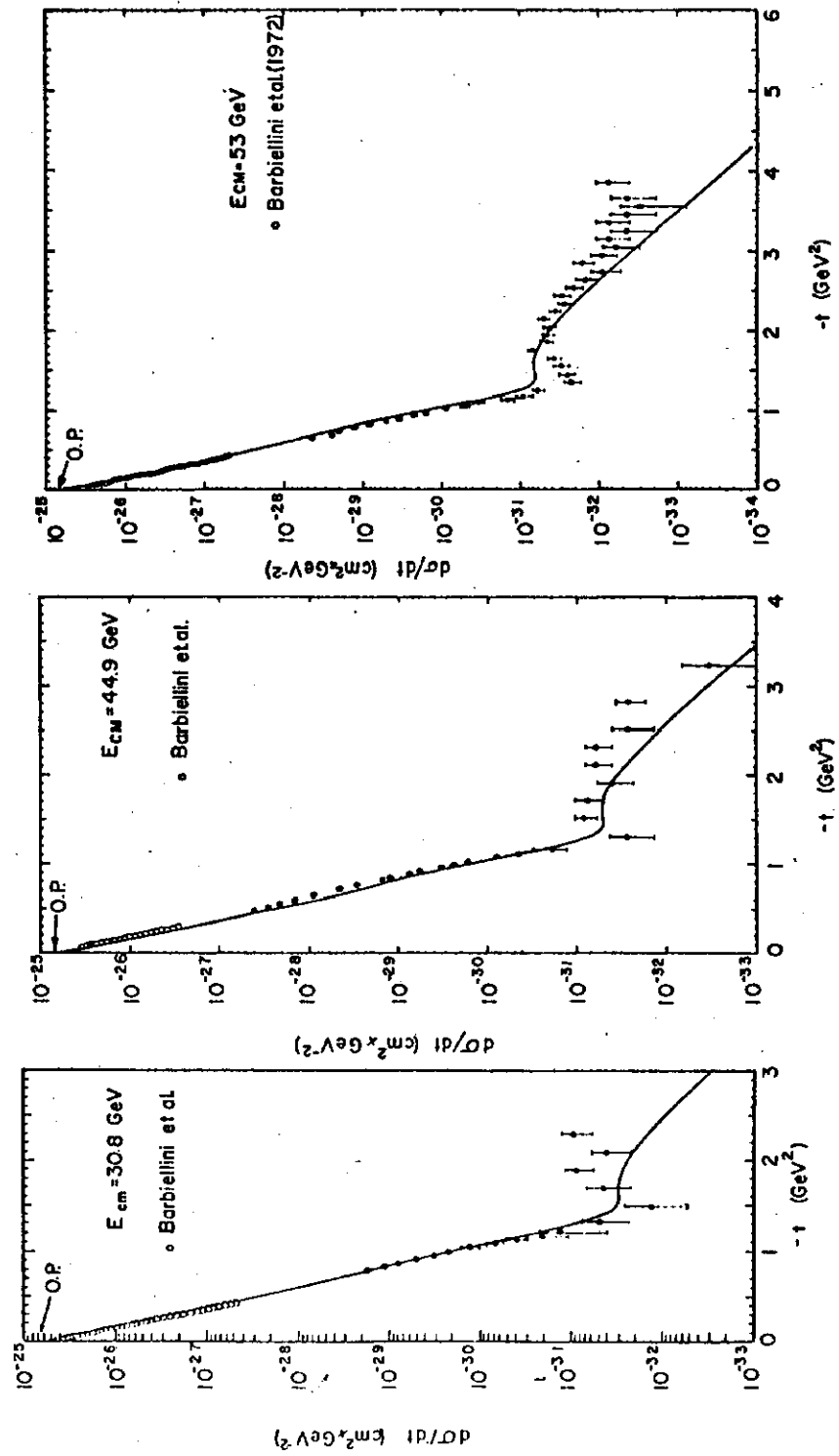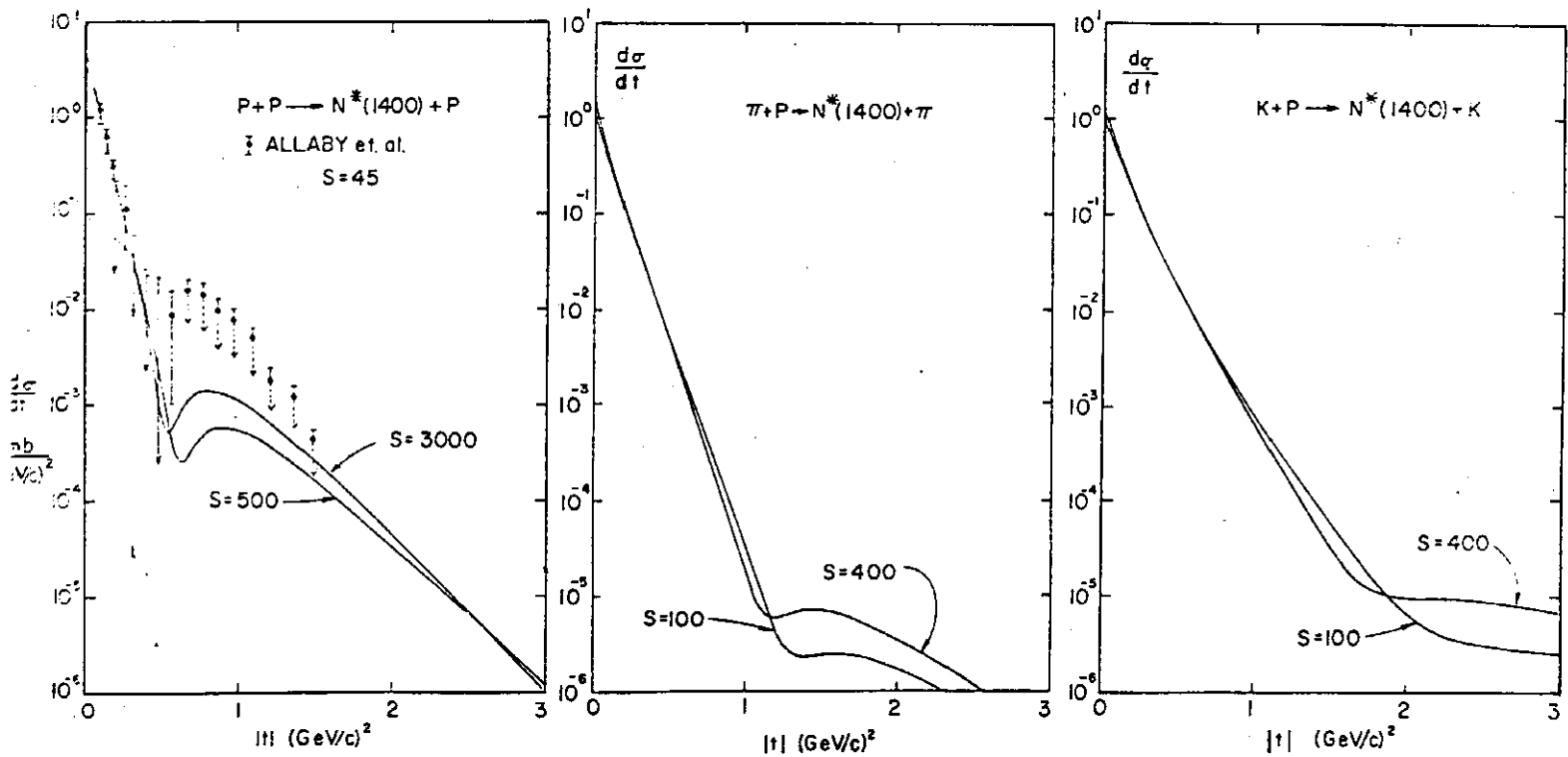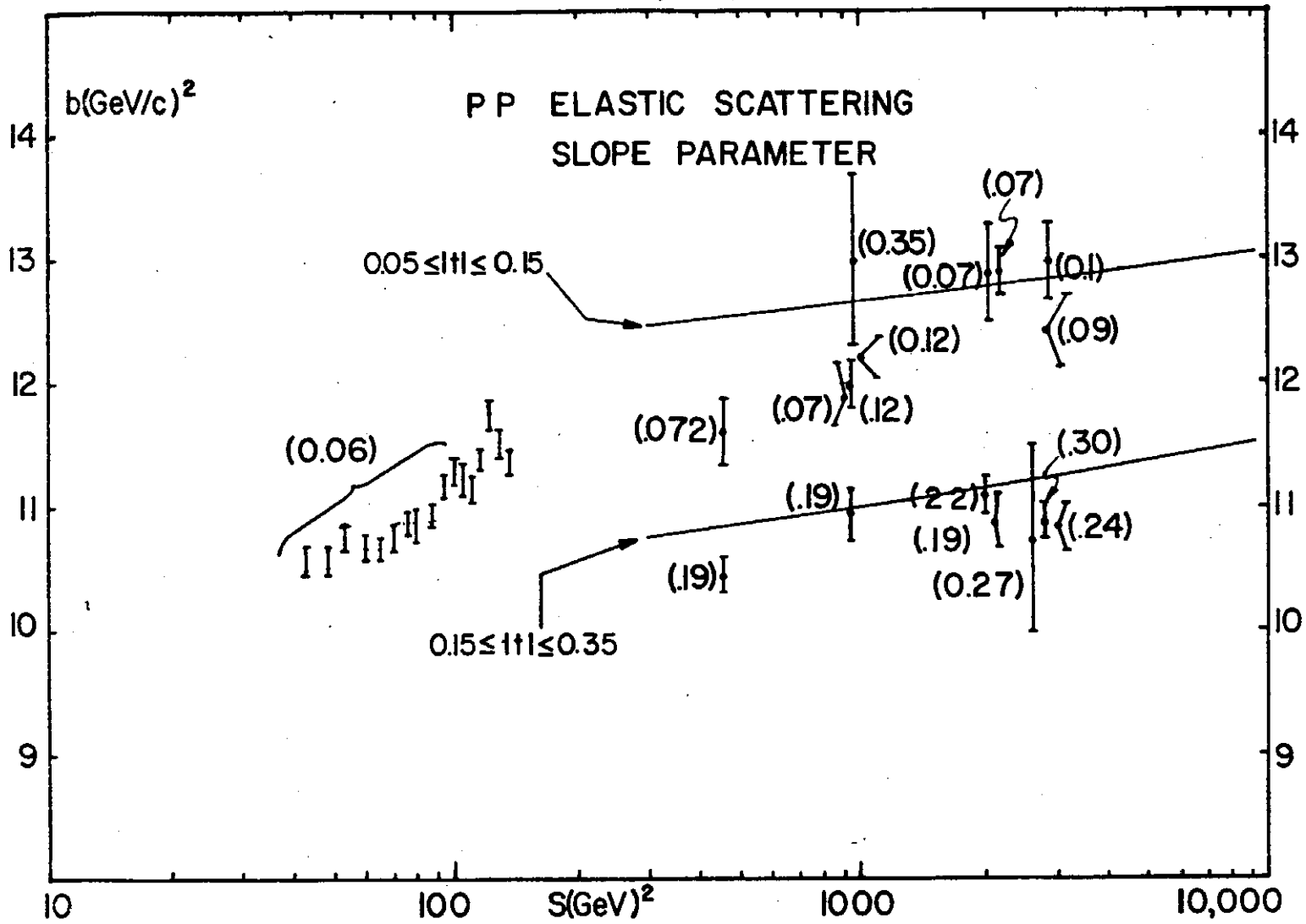for pion production in proton-proton collisions.

Fig. 1

Fig. 2

Fig. 3

P P ELASTIC SCATTERING
SLOPE PARAMETER

b(GeV/c)^2

$0.05 \leq |t| \leq 0.15$

(0.35) (.07) (0.07) (0.1)
(0.12) (.09)
(07) (.12)

(0.06) (.072) (.30)

(.19) (22) (.19) (.24)
(.19) (0.27)

$0.15 \leq |t| \leq 0.35$

S(GeV)^2

P+P ⟶ N*(1400)+P
ALLABY et. al.
S=45

$\frac{d\sigma}{dt}$

$\frac{nb}{(GeV/c)^2}$

S=3000
S=500

|t| (GeV/c)^2

$\frac{d\sigma}{dt}$

π+P ⟶ N*(1400)+π

S=400
S=100

|t| (GeV/c)^2

$\frac{d\sigma}{dt}$

K+P ⟶ N*(1400)+K

S=400
S=100

|t| (GeV/c)^2

Fig. 4

Fig. 5

Fig. 6

PION PROTON
ELASTIC SCATTERING

$\pi^- P$

$\pi^+ P$

α

S(GeV)^2

Fig. 7

KAON PROTON
ELASTIC SCATTERING

$K^- P$

$K^+ P$

α

S(GeV)^2
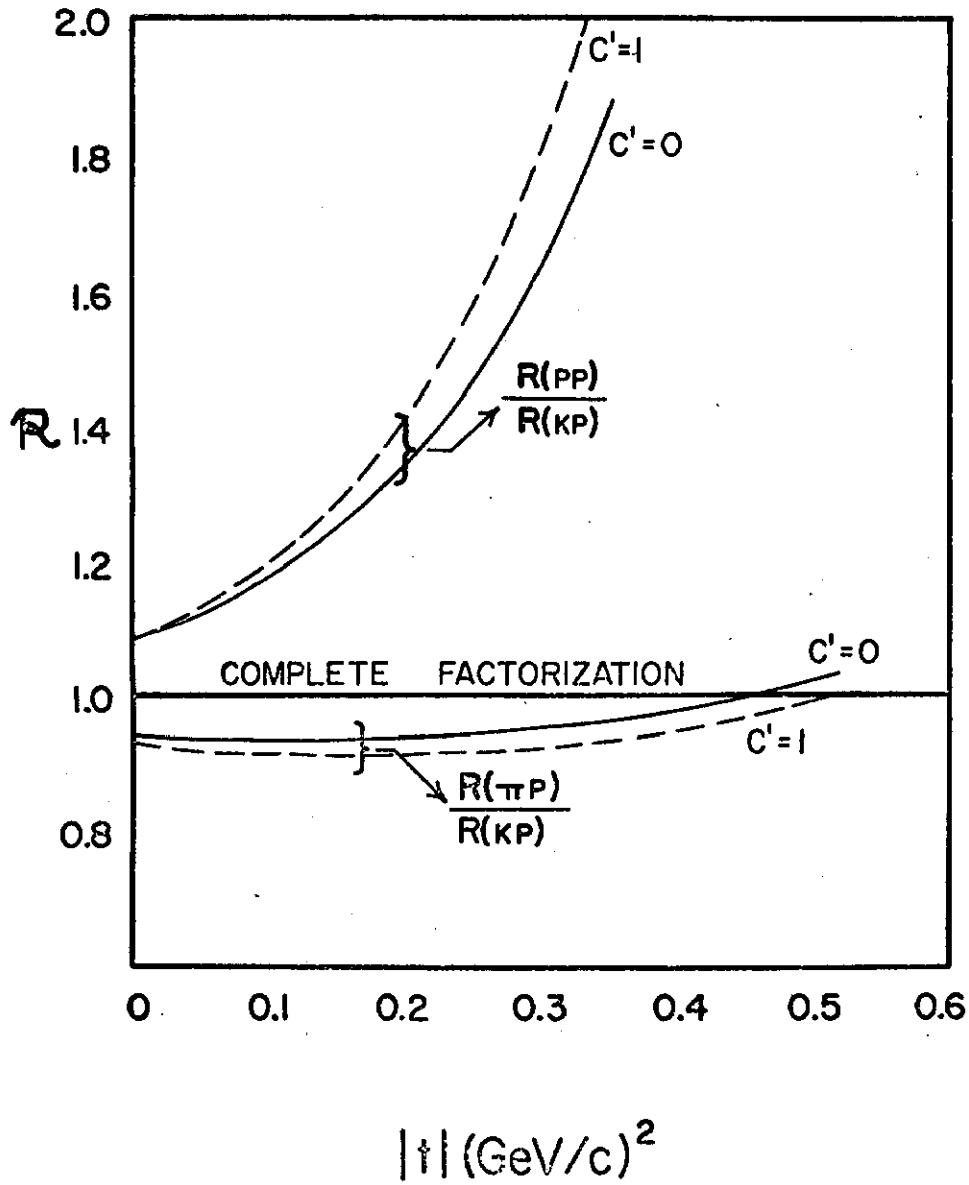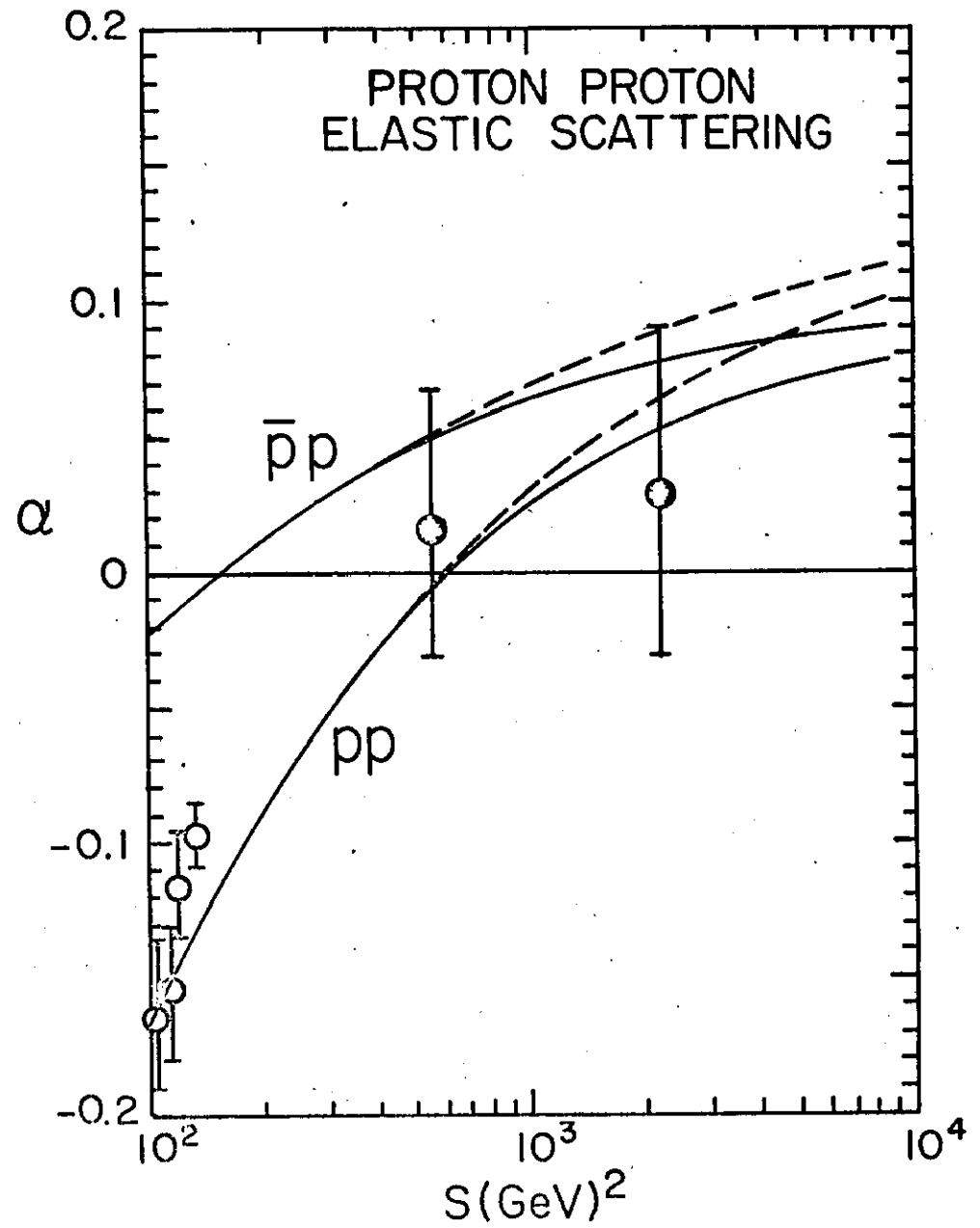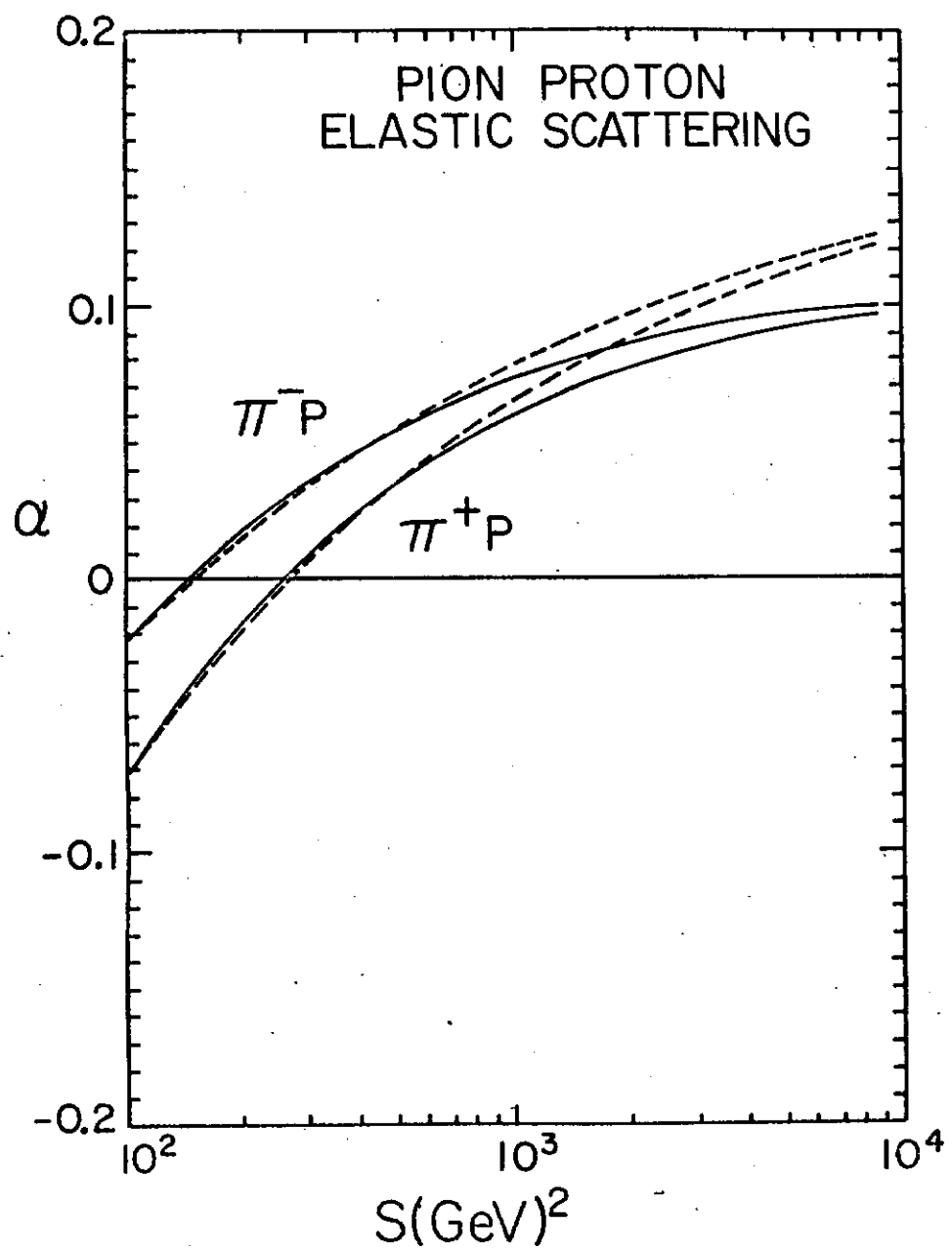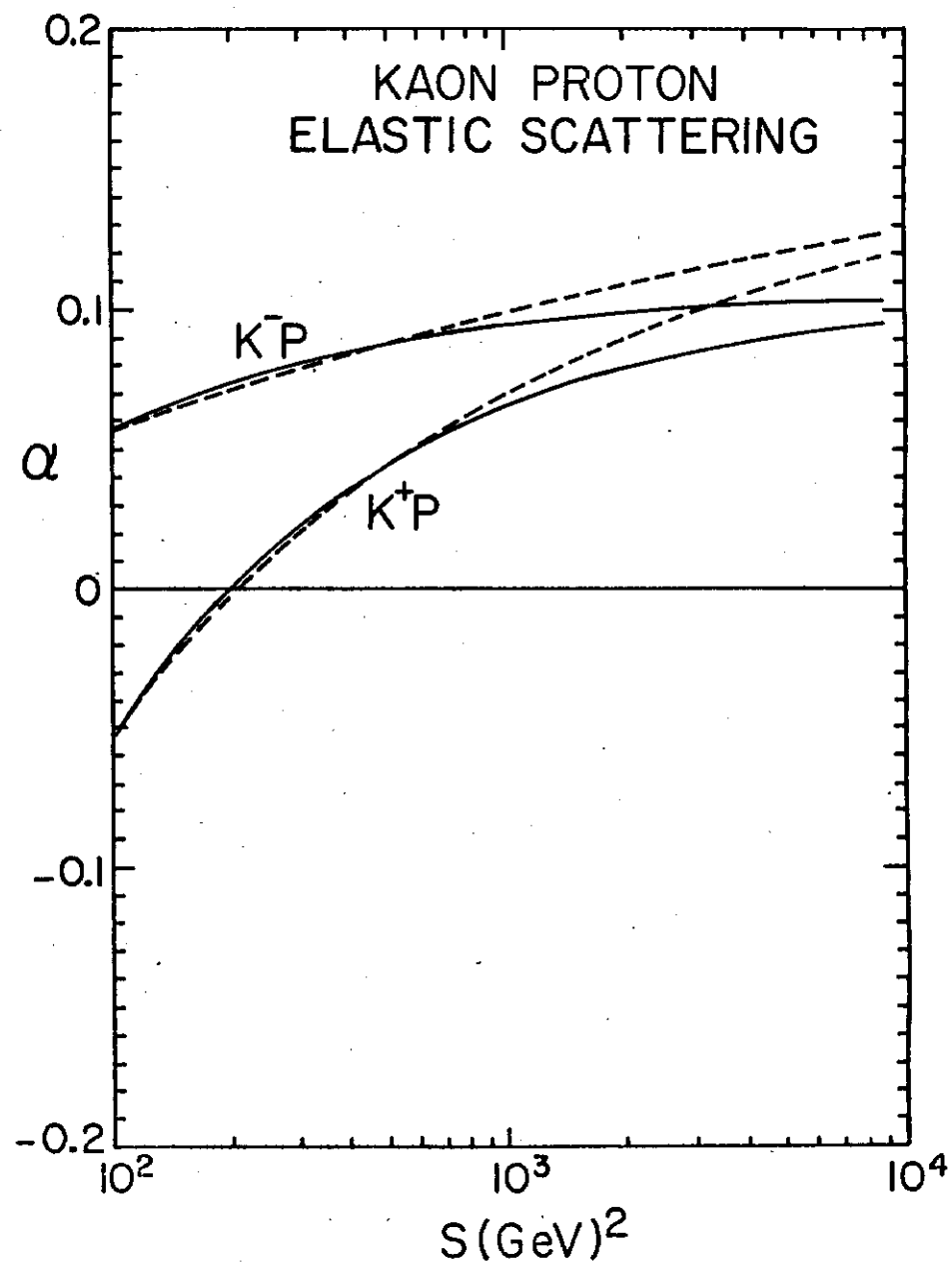
Fig. 8

RAPIDITY PLOT IN THE "CENTRAL" REGION
FOR VARIOUS p_T, FOR π^+ AND π^-

●   SACLAY/STRASBOURG $\pi^{\pm}$
       $s = 910, 2000, 2800 \text{ GeV}^2$

o   BRITISH/SCAND. π^- $s = 2000 \text{ GeV}^2$

+   BRITISH/SCAND. π^+ $s = 2000 \text{ GeV}^2$

Fig. 9

DIFF. CROSS SECTION AT 90° vs s

ISR

PS

◀ SACLAY/STRASBOURG ($\pi^+ + \pi^-$)
   (ALL PART. ESTIMATE)
O   "   (ALL)
●   BARBIELLINI ET AL (ALL)
×   BREINDENBACH ET AL (ALL)
□   NEUHOFER ET AL (I)
⊗   FIDECARO ET AL (I)
▼   MÜCK ET AL   ($\pi^+ + \pi^-$)
■   BØGGILD ET AL (2 × π^-)

$\frac{1}{\sigma_{IN}} \frac{d\sigma}{d\Omega}$ (sr^{-1})

s (GeV^2)

Fig. 10